Analytica Chimica Acta 1221 (2022) 340149

Contents lists available at ScienceDirect

Analytica Chimica Acta

journal homepage: www.elsevier.com/locate/aca

DNA nanomachine activation and Zn^{2+} imaging in living cells with single NIR irradiation

Yuetong Li, Yuxin Xie, Yue Zhang, Hongxia Zhao, Huangxian Ju, Ying Liu *

State Key Laboratory of Analytical Chemistry for Life Science, School of Chemistry and Chemical Engineering, Nanjing University, Nanjing, 210023, PR China

HIGHLIGHTS

- A NIR activatable DNA nanomachine is designed for intracellular Zn^{2+} imaging.
- Single NIR irradiation is used for both DNA nanomachine operation and imaging.
- Multiple emissions of UCNPs are separately used for imaging and internal standard.

GRAPHICAL ABSTRACT

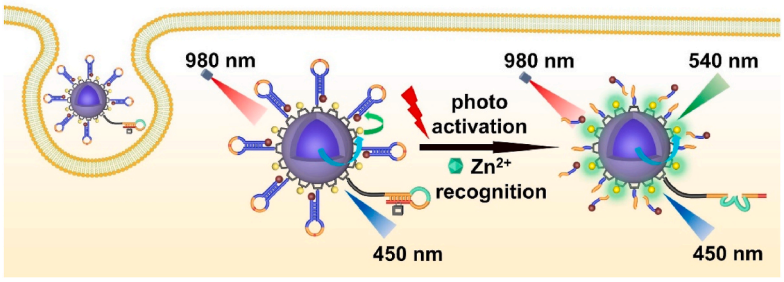

ARTICLE INFO

Keywords:
NIR light activation
Upconversion nanoparticles
DNAzyme
Intracelluar Zn^{2+} imaging
DNA nanomachine

ABSTRACT

Though activatable DNA nanomachines in response to external and internal stimuli successfully improve the temporal and spatial controllability of biosensing and bioimaging, current strategies usually apply different irradiation lights for DNA nanomachine activation and imaging processes. The involvement of short wavelength excitation results in shallow tissue penetration and high background interference. Here we design a photo-locked DNA nanomachine (P-DNA nanomachine) that uses single NIR irradiation for spatiotemporally activating nanomachine operation and metal ion imaging in cancer cells. Upconversion nanoparticles (UCNPs) are modified with energy collector dye FITC, photo-locked DNAzyme and its substrate strands labelled with BHQ1. Part of the UCNPs emission at 450 nm was collected by FITC and quenched by BHQ1 originally. 980 nm irradiation photolyzes PC linker, activates DNAzyme catalytic reaction in the presence of Zn^{2+}, and recovers FITC luminance at 540 nm. The intracellular Zn^{2+} amount was imaged by quantitatively measuring FITC recovery intensity versus internal standard of UCNPs luminance at 450 nm. The presented NIR activatable P-DNA nanomachine demonstrates effective protection against "false positive" signal from extracellular interference, thus has potential application for *in vivo* imaging.

1. Introduction

DNA nanomachine confines DNA reaction strands in nanostructures, and accelerates cascade hybridization reactions in response to tiny stimulus [1–4]. Conjugating DNAzyme catalytic reactions with DNA walkers that move along designed orbits, DNAzyme-based nanomachines could achieve substantial signal enhancement in short time and have become an useful technique for biosensing and bioimaging

* Corresponding author.
E-mail address: yingliu@nju.edu.cn (Y. Liu).

https://doi.org/10.1016/j.aca.2022.340149
Received 30 April 2022; Received in revised form 26 June 2022; Accepted 4 July 2022
Available online 7 July 2022

[5–9].

Most reported DNAzyme-based nanomachines have "always-on" design which automatically operates in response to detection targets as stimuli [10–13]. Though demonstrated satisfactory signal enhancement and detection sensitivity, "always on" DNA nanomachines are susceptible to nonspecific activation by extracellular diffused targets before they arrive desired locations intracellularly, which correspondingly generates "false positive" signal. Designing extra switches, such as lights [14–16], ROS [17] and enzymes [18–20], for DNA nanomachine activation, overcome this barrier by spatiotemporally controlling DNA nanomachine operation. Upconversion nanoparticles (UCNPs) generate UV/Vis emissions upon NIR irradiation, therefore achieved NIR controlled activation and operation of DNA nanomachines [21–25]. However, when apply NIR activatable DNA nanomachines in bioimaging, current approaches mainly relied on the emission of modified fluorophores under short wavelength excitation. The shallow tissue penetration accompanied with high background interference from tissue self-fluorescence limited its further application. Therefore, a DNA nanomachine using single NIR irradiation for both activation and imaging is in urgent need.

Considering the scattered dispersion of activator rare earth ions in UCNPs, the application of their upconversion emissions under NIR irradiation for energy transfer based imaging was difficult [26,27]. Because the energy transfer efficiency between particle internal activator as donor and surface extended acceptor was low due to the long energy transfer distance [28,29]. Our group have developed surface collectors to concentrate upconversion energy at particle surface [30], which improved energy transfer efficiency to surface extended acceptors, and realized miRNA [31], CaB [32] and MMP2 [33] bioimaging under NIR excitation. However, sharing the same NIR irradiation for both DNA nanomachine activation and bioimaging hasn't been achieved up to now. Here we design a photo-locked DNA nanomachine (P-DNA nanomachine) that uses single NIR irradiation for spatiotemporally activating nanomachine and metal ions imaging in cancer cells. Zn^{2+}, as an essential trace element related to many diseases like Alzheimer's disease [34] and other neurodegenerative brain disease [35], is chosen as detection target. Considering the high concentration of free Zn^{2+} in extracellular environments compared with intracellular concentration [36], it is very important to block Zn^{2+} response capability of DNA nanomachine during delivery process and activate it locally in cancer cells for intracellular Zn^{2+} imaging.

To construct NIR activatable P-DNA nanomachine, $NaGdF_4$:Yb, Tm@$NaGdF_4$ UCNPs is modified with surface $–NH_2$ group by ligand exchanging with alendronic acid (ADA), and functionalized with upconversion energy collector dye FITC and NHS-PEG_2-MAL. Photolocked DNAzyme strand (PE-SH) that embedded with a PC linker is subsequently modified on UCNPs surface with its corresponding substrate strands labelled with quencher BHQ1 (S-SH). Part of upconversion luminescence (UCL) of UCNPs at 450 nm under 980 nm excitation is transferred to surface FITC and finally quenched by BHQ1 via two luminance resonance energy transfer (LRET) processes (Scheme 1A). PE-SH has a stable hairpin structure that blocks its reaction activity. After internalization, P-DNA nanomachine is exposed under 980 nm irradiation, which photolyzes PC linker and activates DNAzyme catalytic reaction with substrate S-SH in the presence of Zn^{2+}. The cleavage of BHQ1 labelled substrates drops BHQ1 from UCNPs surface and results in FITC fluorescence recovery at 540 nm under 980 nm excitation (Scheme 1B). It is worth mentioning that the luminescence of UCNPs at 450 nm stayed unchanged during the DNAzyme catalytic reaction, which is used as an internal standard to improve imaging accuracy. As we known, it is the first time to achieve both DNA nanomachine activation and imaging only with 980 nm NIR light irradiation, the avoidance of short wavelength light participation would benefit bioimaging.

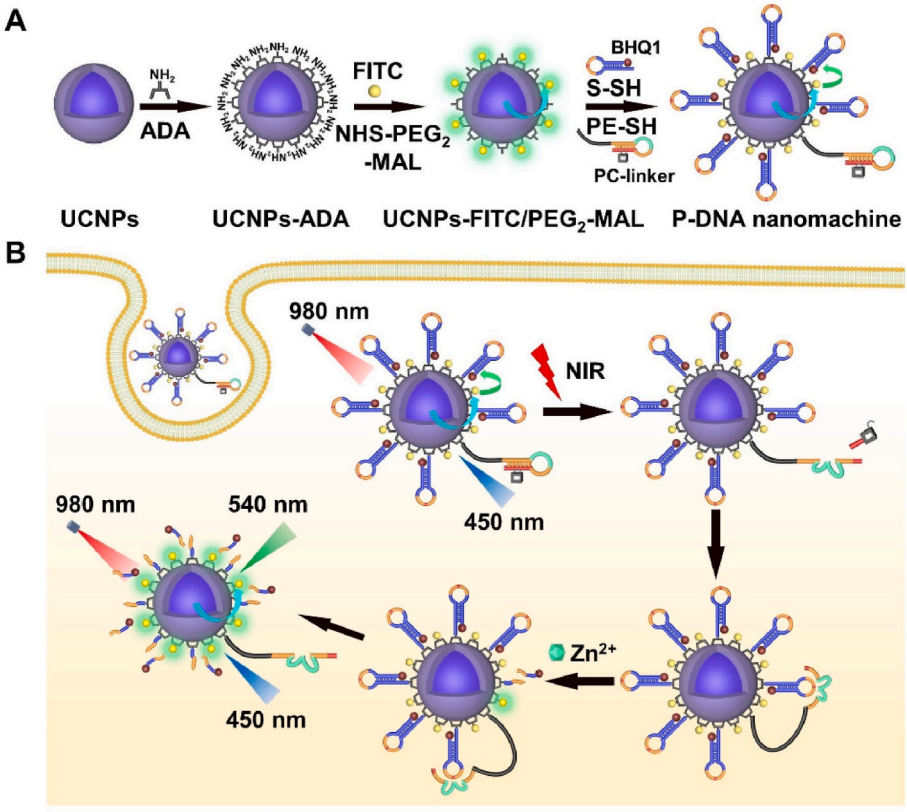

Scheme 1. Schematic illustrations of the working principle of P-DNA nanomachine. (A) construction of P-DNA nanomachine and (B) its activation and intracellular Zn^{2+} imaging upon NIR irradiation.

2. Experimental section

2.1. Fluorescence verification of DNAzyme reaction

All stock solutions of DNA were prepared in 10 mM HEPES buffer (pH 7.4, containing 150 mM NaCl). All DNAs were annealed respectively by heating to 95 °C for 5 min and then slowly cooled to room temperature. 25 nM E, PE and nPE were mixed with 250 nM QS respectively in 10 mM HEPES buffer both in the presence and absence of 50 μM Zn^{2+}. The mixture solutions were irradiated with UV light (7 mW cm^{-2}) for 5 min, and reacted at 37 °C for 1 h. The fluorescence recovery of FAM was recorded at 500–600 nm.

2.2. Polyacrylamide gel electrophoresis (PAGE) analysis

250 nM PE and nPE were mixed with 250 nM S respectively in 10 mM HEPES buffer both in the presence and absence of 50 μM Zn^{2+}. The mixture solutions were irradiated with UV light (7 mW cm^{-2}) for 5 min, and reacted at 37 °C for 1 h. To perform PAGE analysis, 5 μL of the reaction sample was mixed with 1 μL 6 × loading buffer and loaded into 10% native polyacrylamide gel, followed by implemented at 120 mV for 90 min in 1 × TBE buffer. After that, the gel was stained with SYBR Gold for 30 min and used for imaging analysis via a Bio-Rad fluorescence gel imaging system.

2.3. Preparation of P-DNA nanomachine

2.3.1. Preparation of UCNPs-ADA

UCNPs surface ligand OA was exchanged with ADA to transfer them from $CHCl_3$ to aqueous solution. 200 mg of the above prepared UCNPs was dispersed in 10 mL $CHCl_3$, mixed with 4 mL ethanol and 6 mL ADA aqueous solution. The pH of the mixture solution was adjusted to 2–3 with 1 M HCl. The mixture solution was ultrasonicated for 15 min and stirred for 2 h, UCNPs-ADA was obtained in the upper aqueous solution, washed with ethanol/deionized water three times and re-dispersed in DMF.

2.3.2. Preparation of UCNPs-FITC/PEG_2-Mal

FITC and NHS-PEG_2-Mal were covalently conjugated to UCNPs-ADA via surface –NH_2 groups. 300 μM FITC or FITC/NHS-PEG_2-Mal mixture with various molar ratios (1:20, 1:15, 1:10, 1:7, 1:5) were added into 1.0 mg UCNPs-ADA in DMF. After stirring overnight, the as-obtained UCNPs-FITC/PEG_2-Mal was centrifuged, washed with HEPES buffer for three times and re-dispersed in HEPES buffer. The number of FITC modified on particle surface was quantified according to FITC standard curve.

2.3.3. Preparation of P-DNA nanomachine

PE-SH and nPE-SH were annealed respectively by heating to 95 °C for 5 min and slowly cooled to room temperature. The disulfide bond of thiol terminus DNA strands was cleaved by treatment with TCEP at pH 5.0 for 1 h, then purified with 3 k Amicon tube. Subsequently, 10 μM PE-SH and 10 μM S-SH were mixed at different molar ratio with total volume of 200 μL, added with 1.0 mg UCNPs-FITC/PEG_2-Mal in HEPES buffer and reacted for 12 h. The as-obtained P-DNA nanomachine was centrifuged, washed with HEPES buffer and stored at 4 °C. To measure the number of DNA strands on each UCNP, TAMRA labelled S-SH and PE-SH were reacted with UCNP-FITC/PEG_2-Mal according to the same procedure, and the number of DNA strands modified on UCNPs surface was quantified by measuring TAMRA fluorescence intensity according to TAMRA-DNA calibration curve. To prepare N-DNA nanomachine and A-DNA nanomachine, nPE-SH and E-SH were used respectively instead of PE-SH.

2.4. In vitro detection of Zn^{2+}

100 μL 0.2 mg mL^{-1} P-DNA nanomachine was irradiated with 980 nm light (1 W cm^{-2}) for 20 min, added with 100 μL Zn^{2+} of various concentrations (1, 2, 3, 4, 5, 7.5, 10, 15, 25, 50, 100, 200 μM). Incubated at 37 °C for 2 h, and the recovery of FITC fluorescence intensity was measured at 540 nm under 980 nm excitation. As the internal standard luminance, the luminance intensity of UCNPs was measured at 450 nm. The Zn^{2+} concentration was fixed at 50 μM, and control experiments were performed with A-DNA nanomachine and N-DNA nanomachine with the same procedure respectively. The reaction specificity of P-DNA nanomachine was tested among other metal ions, including 1 mM Ca^{2+}, K^{+}; 50 μM Cd^{2+}, Fe^{2+}, Mg^{2+}, Cu^{2+}, Fe^{3+}, Cr^{3+}.

2.5. Intracellular imaging of Zn^{2+}

HeLa cells (1×10^5) were plated in a confocal dish and grown to 70% confluence. 200 μL DMEM containing 100 μg mL^{-1} P-DNA nanomachine was added to each well and incubated for 6 h. After washing with PBS for three times, the cells were irradiated with 980 nm light (1 W cm^{-2}) for 20 min (5 min break after 5 min irradiation). Subsequently, the cells were further treated with 50 μM Zn^{2+} and pyrithione in 1:2molar ratio for 30 min and incubated for another 2 h. After washing with PBS, cells were imaged by TCS SP5 CLSM with 63x oil objective. FITC luminescence recovery at 500–550 nm under 980 nm excitation was collected as Zn^{2+} imaging signal, and UCNPs emission at 430–500 nm was also collected as internal standard signal. Control experiments were performed with the same procedure, N-DNA nanomachine and A-DNA nanomachine were used instead of P-DNA nanomachine respectively.

2.6. ICP-OES quantification of intracellular Zn^{2+}

HeLa cells were cultured in DMEM for 24 h, and treated with different concentrations of Zn^{2+} (10, 25, 50 μM) and pyrithione in 1:2molar ratio for 30 min. The treated cells were then detached by 0.25% trypsin-EDTA and re-suspended in 1.0 mL PBS. Cell numbers were determined with Countess® II FL automated cell counter. The cells were then collected in centrifuge tubes and digested in 0.3 mL HNO_3 at 70 °C for 3 h. The final samples were diluted to 3 mL with ultrapure water and analyzed for total zinc content by ICP-OES.

3. Results and discussion

3.1. Design of photo-locked DNAzyme and its response to Zn^{2+}

Photo-locked DNAzyme strand (PE) was designed by extending 8-17E DNAzyme with 11 base blocking section (BS) at 5' terminus. BS kept PE in a hairpin structure, thus hindered the formation of active secondary structure of DNAzyme. Self-quenched substrate strand (QS) was designed by labelling FAM and its corresponding quencher BHQ1 at two terminals of substrate strand (S) respectively, which has close distance within a hairpin structure. A photo-cleavable (PC) linker was embedded in BS, which was photolyzed upon UV irradiation and led to the dropping of partial BS to convert PE into active DNAzyme strand (E) (Fig. 1A). Activated PE cleaved QS into BHQ1 labelled S1 and FAM labelled S2 in the presence of Zn^{2+} with obvious FAM fluorescence recovery (Fig. 1B, UV(+) Zn^{2+}(+); UV(+) Zn^{2+}(−)). FAM fluorescence recovery intensity from UV-activated PE was comparable to that from QS cleaved by E in response to Zn^{2+} (Fig. 1C, E, Zn^{2+}(+); E, Zn^{2+}(−)), indicating the efficient activation of PE by UV exposure. On the contrary, PE showed very low FAM fluorescence in response to Zn^{2+} in the absence of UV exposure (Fig. 1B, UV(−) Zn^{2+}(+)), demonstrating the satisfactory activity inhibition from BS in PE. As a negative control, nPE with the same sequence as PE but in the absence of PC linker, was treated with UV exposure and challenged with Zn^{2+}, which barely showed FAM fluorescence recovery (Fig. 1C, nPE, UV(+) Zn^{2+}(+)).

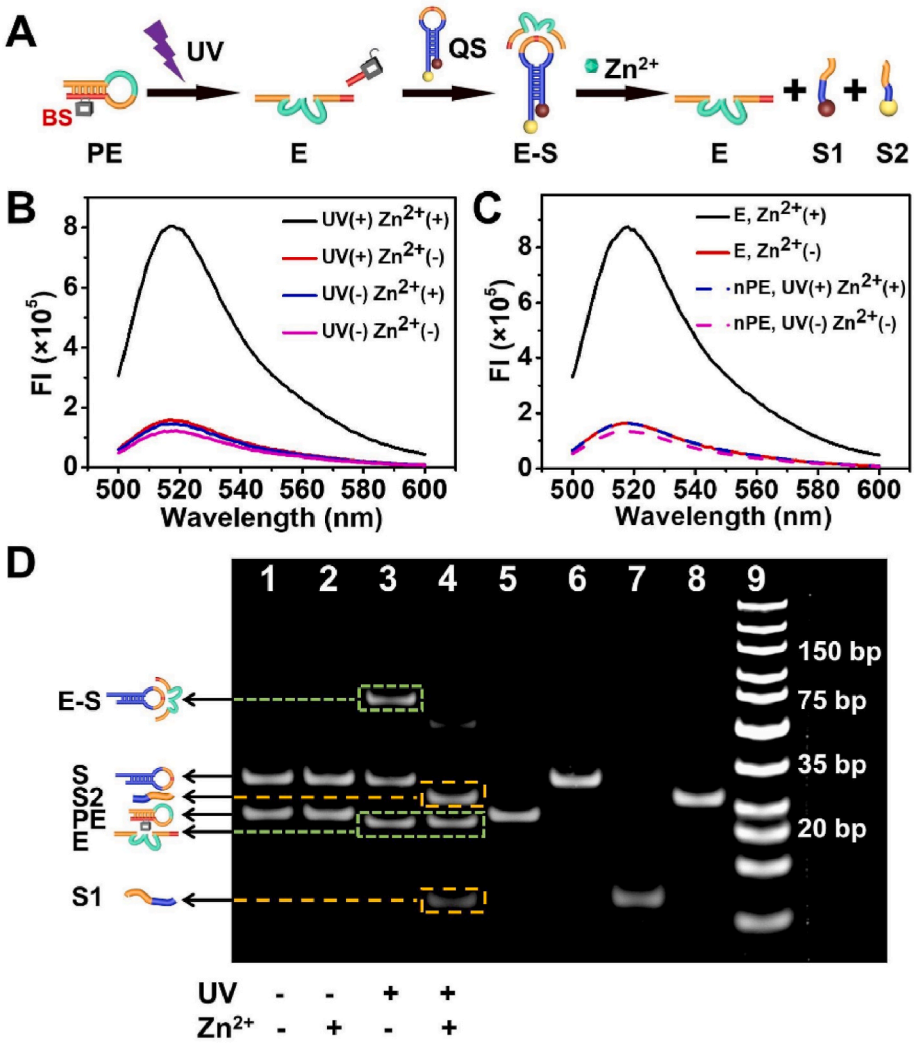

Fig. 1. *In vitro* verification of DNA strands to Zn^{2+} (A) Schematic illustration for photo activation of PE and subsequent DNAzyme catalytic reaction with QS in response to Zn^{2+}. Fluorescence spectra of (B) PE and QS mixture under different reaction conditions in the presence/absence of UV exposure and Zn^{2+}, and (C) E and QS mixture in the presence/absence of Zn^{2+}, nPE and QS mixture in the presence/absence of UV exposure and Zn^{2+}. (D) Native PAGE of PE and S mixture under different reaction conditions (lane 1–4), lane 1: UV(−) Zn^{2+} (−), lane 2: UV(−) Zn^{2+} (+), lane 3: UV(+) Zn^{2+} (−), lane 4: UV(+) Zn^{2+} (+); individual bands (lane 5–8), lane 5: PE, lane 6: S, lane 7: S1, lane 8: S2; lane 9: DNA ladder.

The photo activation of PE and its corresponding response to Zn^{2+} was further confirmed by polyacrylamide gel electrophoresis (PAGE) experiments. UV irradiation generated a new band in PAGE with the same mobility as that of E, indicating the successful activation of PE. The dropping segment was not observed in PAGE due to its short length of only 6 nt (Figure. S1A). Simply mixing PE and S in the absence of UV exposure demonstrated two separate bands at their corresponding positions, even in the presence of Zn^{2+} (Fig. 1D, lane 1 and 2). UV irradiation cleaved PE, and demonstrated complete disappearance of PE band and the appearance of two new bands: one with slight higher mobility than PE indicating E generation, the other with lower mobility indicating the successful generation of E-S complex (Fig. 1D, lane 3). The subsequent addition of Zn^{2+} resulted in the disappearance of E-S complex band, in accompany with the appearance of two new bands at S1, S2 corresponding positions. The $(T)_8$ tail located in 3' terminus of S2 resulted in its lower migration rate compared with S1. (Fig. 1D, lane 4). This result confirmed the photo activation of PE and its response to Zn^{2+}. As a negative control, nPE in the absence of PC linker was also incubated with S, which always demonstrated two separate bands regardless of the existence of UV exposure or Zn^{2+} addition (Figure. S1B).

3.2. Construction and characterization of P-DNA nanomachine

Core-shell structured UCNPs ($NaGdF_4$:49%Yb,1%Tm@$NaGdF_4$) was synthesized according to a previous approach reported by our group [37]. TEM images showed uniform hexagonal shape for the as-obtained UCNPs core with 19.9 ± 0.98 nm and UCNPs with 24.5 ± 1.2 nm (Fig. 2A). The UCNPs core $NaGdF_4$:49%Yb,1%Tm demonstrated upconversion luminescence (UCL) peaks at 345, 365, 450 and 475 nm corresponding to $^1I_6 \rightarrow {}^3F_4$, $^1D_2 \rightarrow {}^3H_6$, $^1D_2 \rightarrow {}^3F_4$ and $^1G_4 \rightarrow {}^3H_6$ transitions of Tm^{3+} [38]. The coating of inert shell $NaGdF_4$ prevented surface-induced quenching of UCL and led to 5 times intensity enhancement (Fig. 2B). ADA, a bidentate ligand with amine terminus group, was used to replace UCNPs original ligand OA to increase their water dispersity and facilitate further functionalization. The appearance of ADA characteristic peak at 1020 cm^{-1} (P═O stretching vibration) in accompany with the disappearance of OA characteristic peak at 2925 cm^{-1} (–CH_2– stretching vibration) in FTIR spectra confirmed the successful surface ligand exchange process (Fig. 2C, line 1 and 2). Compared with UCNPs, the as-obtained UCNPs-ADA slightly increased zeta potential from 28.2 ± 1.2 mV to 40.0 ± 2.1 mV due to surface functionalized amine group and hydrodynamic size from 30.4 ± 4.2 nm to 37.7 ± 1.1 nm (Figs. 2D, 1 and 2).

FITC was then conjugated to UCNPs-ADA by reacting with the amine group, and acted as surface collector to concentrate the scattered emission energy from interior UCNPs to particle surface [30]. To facilitate the further conjugation of DNA strands on UCNPs surface, NHS-PEG_2-Mal was also co-immobilized on the UCNPs-ADA surface. The successful modifications of FITC and NHS-PEG_2-Mal demonstrated amide characteristic peak at 1670 cm^{-1} (C═O stretching vibration) in FTIR spectra (Fig. 2C, line 3). The absorption band of FITC in the range of 400–500 nm (Fig. 2E, dash line 2) overlapped well with the emission

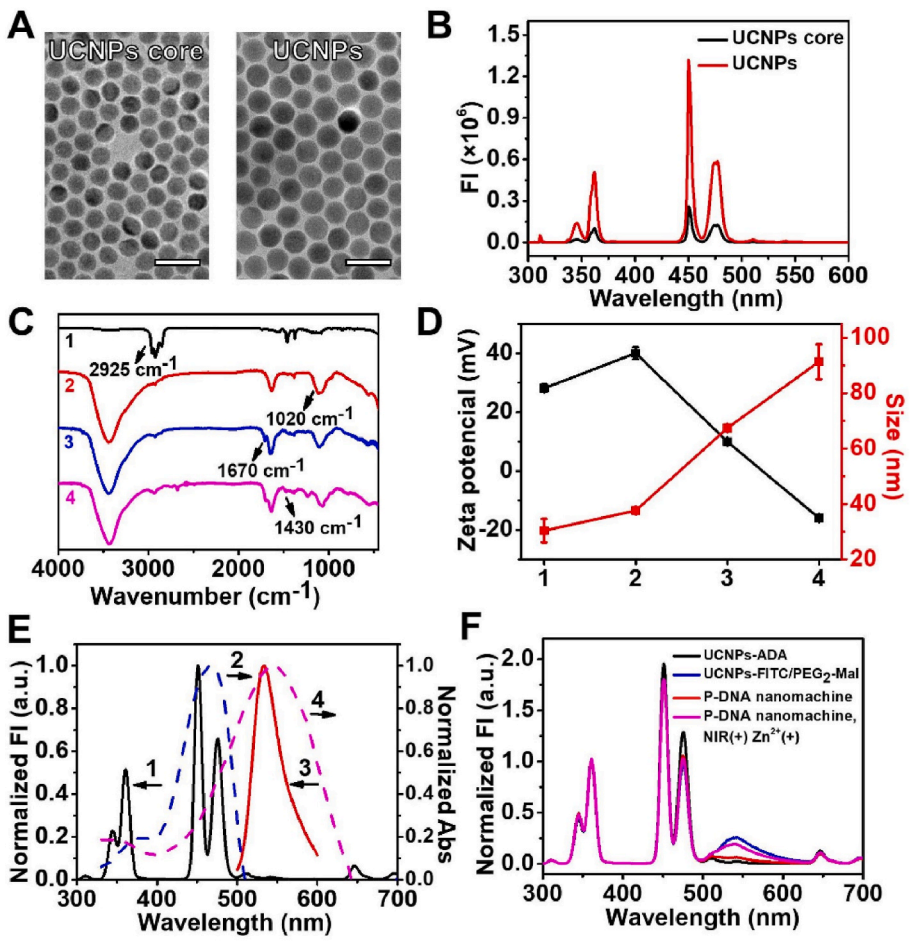

Fig. 2. Characterization of P-DNA nanomachine. (A) TEM images and (B) upconversion luminance spectra of UCNPs core $NaGdF_4$:Yb, Tm and UCNPs $NaGdF_4$: Yb,Tm@$NaGdF_4$ (scale bar: 50 nm). (C) FTIR spectra and (D) Zeta potential/hydrodynamic sizes of (1) UCNPs, (2) UCNPs-ADA, (3) UCNPs-FITC/PEG_2-Mal and (4) P-DNA nanomachine. Data are represented as means ± SD (n = 3). (E) Normalized fluorescence emission spectra (solid lines) of (1) UCNPs under 980 nm excitation and (3) FITC under 488 nm excitation, and normalized absorption spectra (dashed lines) of (2) FITC and (4) BHQ1. (F) Normalized upconversion luminance spectra of UCNPs-ADA, UCNPs-FITC/PEG_2-Mal, P-DNA nanomachine, and P-DNA nanomachine in response to NIR exposure and Zn^{2+} (P-DNA nanomachine, NIR(+) Zn^{2+}(+)).

peak of UCNPs at 450 and 475 nm (Fig. 2E, solid line 1). Therefore, the as-obtained UCNPs-FITC/PEG_2-MAL demonstrated energy transfer from UCNPs to FITC with an obvious emission peak at 540 nm under 980 nm excitation (Fig. 2F, UCNPs-FITC/PEG_2-MAL). The molar ratio of FITC over NHS-PEG_2-Mal was optimized, and achieved the highest FITC luminance intensity at 1:7. The continuous increase of FITC percentage suppressed its luminance intensity due to aggregation-caused quenching (ACQ) effect [39] (Figure. S2A, B). The number of surface modified FITC

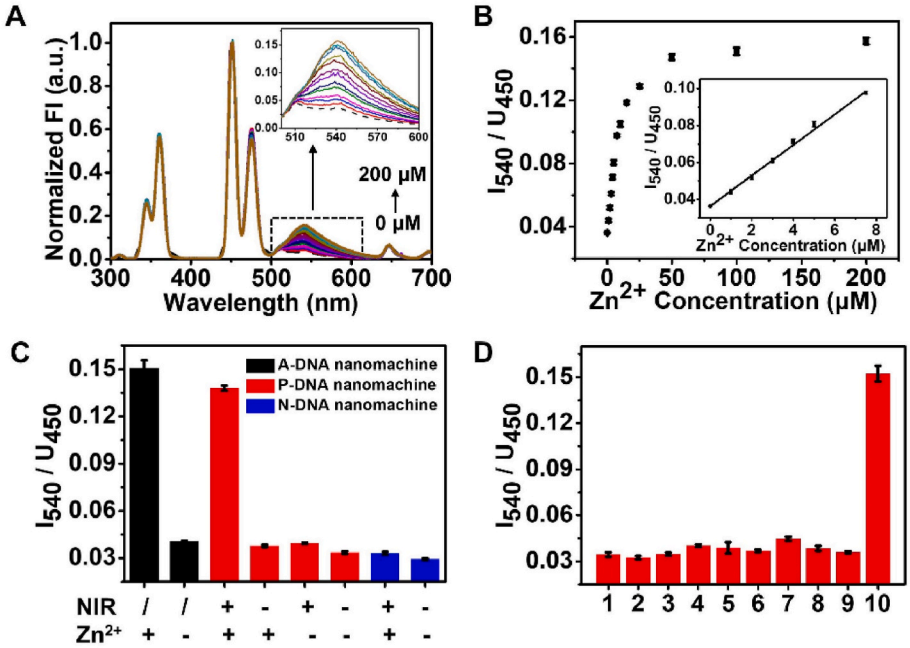

Fig. 3. *In vitro* application of P-DNA nanomachine to Zn^{2+}. (A) Fluorescence spectra and (B) corresponding intensity ratio of FITC emission at 540 nm over UCNPs luminance at 450 nm (I_{540}/U_{450}) for P-DNA nanomachine in response to Zn^{2+} concentrations (0, 1, 2, 3, 4, 5, 7.5, 10, 15, 25, 50, 100, 200 μM). Inset shows the calibration curve for Zn^{2+}. (C) I_{540}/U_{450} for A-DNA nanomachine (black columns), P-DNA nanomachine (red columns) and N-DNA nanomachine (blue columns) under different reaction conditions. (D) I_{540}/U_{450} for NIR activated P-DNA nanomachine (1) and NIR activated P-DNA nanomachine in response to 1 mM K^+ (2); 1 mM Ca^{2+} (3); 50 μM Cu^{2+} (4); 50 μM Cd^{2+} (5); 50 μM Fe^{2+} (6); 50 μM Mg^{2+} (7); 50 μM Cr^{3+}(8); 50 μM Fe^{3+} (9); 50 μM Zn^{2+} (10). Data are represented as means ± SD (n = 3). (For interpretation of the references to colour in this figure legend, the reader is referred to the Web version of this article.)

was calculated according to FITC standard calibration curve to get 126 ± 5 FITC per particle (Figure. S2C, D). Zeta potential of UCNP-FITC/-PEG_2-Mal was dropped to 10.0 ± 0.14 mV due to the occupied amine functional groups with an increase of hydrodynamic size to 67.4 ± 0.8 nm (Figs. 2D and 3).

Thiol terminus photo-locked DNAzyme strand (PE-SH) and its corresponding substrate strand labelled with quencher BHQ1 (S-SH) were then covalently conjugated to UCNPs-FITC/PEG_2-Mal through thiol and maleimide reaction to complete P-DNA nanomachine. The as-obtained DNA nanomachine showed negative zeta potential of −15.9 ± 0.61 mV due to negatively charged DNA strands, increased hydrodynamic size to 91.4 ± 6.3 nm (Figs. 2D and 4), and demonstrated DNA characteristic absorption at 260 nm in the UV–Vis absorption spectra (Figure. S3) and 1430 cm^{-1} (glucosidic bond stretching vibration) in FTIR spectra (Fig. 2C, line 4). BHQ1 maximum absorption band at 550 nm (Fig. 2E, dash line 4) overlapped well with FITC emission peak at 540 nm (Fig. 2E, solid line 3), which acted as an energy transfer acceptor that completely suppressed FITC emission (Fig. 2F, P-DNA nanomachine). This achieved the successful 450 nm UCL from UCNPs to surface extended quencher BHQ1 under 980 nm excitation, which guaranteed the application of P-DNA nanomachine in subsequent Zn^{2+} detection.

3.3. *In vitro response of P-DNA nanomachine to Zn^{2+}*

UCNPs generated UCL at 365 nm under 980 nm irradiation and activated DNAzyme catalytic reaction in the presence of 50 μM Zn^{2+}, resulted in the recovery of the FITC luminance at 540 nm. The recovered FITC luminance intensity was comparable to that of UCNPs-FITC/PEG_2-MAL, indicating the sufficient reaction of DNAzyme with substrate (Fig. 2F, P-DNA nanomachine, NIR(+) Zn^{2+}(+)). Meanwhile, the 450 nm of UCNPs emission, which was attributed to the emission from Tm^{3+} located interior of particle that didn't participate in LRET process, remained unchanged during FITC luminance recovery. It act as an internal standard in Zn^{2+} detection. To optimize the response sensitivity of P-DNA nanomachine to Zn^{2+}, PE-SH/S-SH mixtures with various molar ratios were immobilized on UCNPs surface, and achieved lowest background signal with maximized FITC signal recovery at 1:10molar ratio of PE-SH/S-SH (Figure. S4A, B). Compared with fluorescence of $UCNP_S$-FITC/PEG_2-Mal in the absence of BHQ1, FITC quenching efficiency was calculated as ~85% for P-DNA nanomachine. TAMRA labelled substrate strand (TAMRA-S-SH) was used to calculate the number of substrate strand on UCNPs surface, which was determined as 106 ± 2 TAMRA-S-SH per UCNP according to TAMRA-DNA calibration curve (Figure. S4C, D).

To verify the *in vitro* application of P-DNA nanomachine in Zn^{2+} detection, it was exposed under NIR irradiation and challenged with different concentrations of Zn^{2+} from 0 to 200 μM. FITC fluorescence recovery gradually increased according to Zn^{2+} concentration (Fig. 3A), and the intensity ratios of FITC emission at 540 nm over UCNP luminance at 450 nm (I_{540}/U_{450}) demonstrated a linear correlation in Zn^{2+} concentration range from 1 to 7.5 μM with a limit of detection (LOD) of 94.8 nM (Fig. 3B). The response sensitivity of P-DNA nanomachine was comparable to that of the "always active" DNA nanomachine (A-DNA nanomachine) which was modified with E-SH instead of PE-SH (Fig. 3C, black and red columns), indicating the efficient photo activation. In the absence of NIR irradiation, FITC fluorescence in response to 50 μM Zn^{2+} remained similar to background (Fig. 3C, red columns), indicating the effective blocking of P-DNA nanomachine against "false positive" signal. Non-active DNA nanomachine (N-DNA nanomachine), which was modified with nPE-SH in the absence of PC linker instead of PE-SH, was used as negative control. It showed little FITC recovery even in the presence of NIR irradiation and additional Zn^{2+} (Fig. 3C, blue columns), indicating little interference from environmental factors. To verify the reaction specificity, P-DNA nanomachine was challenged with various biologically relevant metal ions. All the ions demonstrated little FITC recovery compared to background signal except Zn^{2+} (Fig. 3D). The good reaction specificity of P-DNA nanomachine makes it appropriate for Zn^{2+} sensing in the complex biological system.

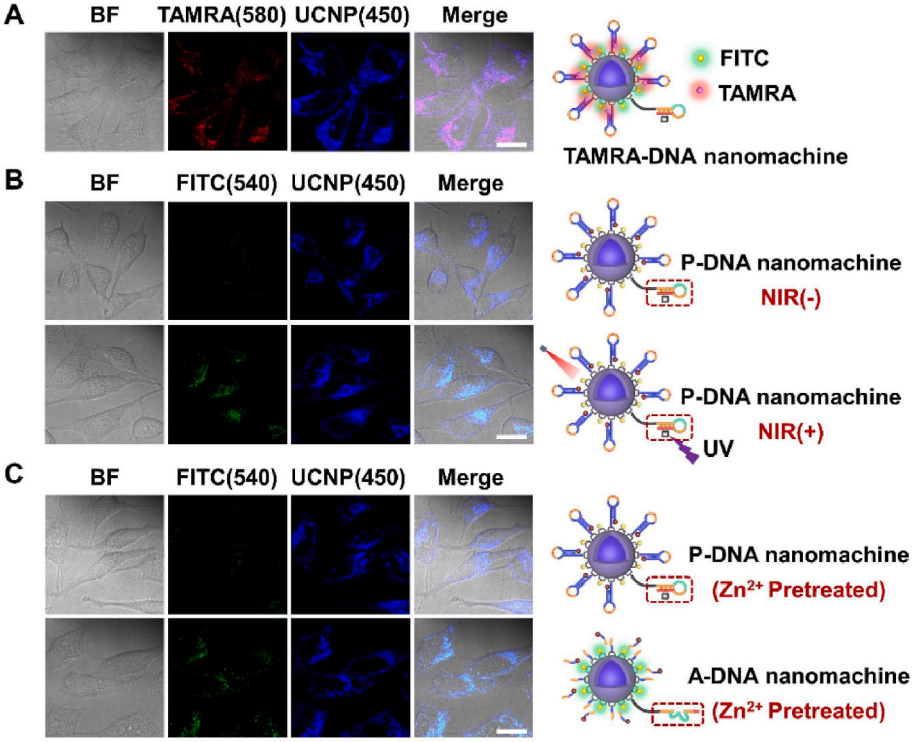

Fig. 4. Intracellular imaging of Zn^{2+} via P-DNA nanomachine. CLSM images of (A) HeLa cells incubated with TAMRA-DNA nanomachine, (B) Zn^{2+} treated HeLa cells incubated with P-DNA nanomachine in the presence and absence of NIR irradiation and (C) HeLa cells incubated with *in vitro* Zn^{2+} pretreated P-DNA nanomachine and Zn^{2+} pretreated A-DNA nanomachine (scale bar: 20 μm).

3.4. P-DNA nanomachine for intracellular Zn^{2+} imaging

The biocompatibility of P-DNA nanomachine and cytotoxicity of corresponding treatment were evaluated with MTT assay. HeLa cells still kept more than 91.7% of viability even at 200 μg mL^{-1} DNA nanomachine treatment both in the presence and absence of NIR irradiation (Figure S5A), and the additional Zn^{2+} treatment at different concentrations also showed no significant cytotoxicity (Figure. S5B). The good biocompatibility of P-DNA nanomachine make it appropriate for intracellular application.

To verify the application of P-DNA nanomachine for NIR activated Zn^{2+} imaging in living cells, HeLa cell was chosen as the model cell and incubated with TAMRA labelled DNA nanomachine (TAMRA-DNA nanomachine) for 6 h, which demonstrated bright intracellular TARMA fluorescence at 580 nm, indicating the efficient intracellular delivery of DNA nanomachine. Intracellular TAMRA fluorescence also perfectly overlapped with UCNPs luminance at 450 nm in CLSM images, indicating the integrity of DNA nanomachine during internalization process (Fig. 4A). Colocalization experiment was performed with DNA nanomachine-FITC prepared with substrate S-SH' in the absence of BHQ1, which showed FITC fluorescence all the time. Clear separation of FITC fluorescence (green) and Lyso-tracker red fluorescence (red) was observed after 6 h incubation, indicating the successful lysosome escape of DNA nanomachine (Figure. S6).

P-DNA nanomachine loaded HeLa cells were then exposed under NIR irradiation to activate DNAzyme and further treated with 50 μM Zn^{2+} and pyrithione to increase the intracellular concentration of Zn^{2+} [15,16]. With NIR irradiation, the intracellular FITC fluorescence showed a gradual recovery over time and saturated at 2 h (Figure. S7, Fig. 4B, NIR (+)), indicating the successful intracellular response to Zn^{2+}. There was little FITC recovery in the absence of NIR irradiation even with additional Zn^{2+}, indicating the successful block of DNAzyme (Fig. 4B, NIR (−)). Considering the very low concentration of free Zn^{2+} intracellularly [36], FITC fluorescence was barely observed from HeLa cells without Zn^{2+} loading whether with NIR irradiation or not (Figure. S8). N-DNA nanomachine was used as negative control, which showed little FITC recovery even in the presence of NIR irradiation and additional Zn^{2+} (Figure. S9). The unchanged UCNPs emission at 450 nm under 980 nm excitation acted as an appropriate internal standard to improve the accuracy of intracellular imaging. To further demonstrate the capability of P-DNA nanomachine protecting against "false positive" signal from extracellular interference, P-DNA nanomachine and A-DNA nanomachine were pretreated with 50 μM Zn^{2+} for 2 h *in vitro* separately, simulating the nonspecific activation during the systemic circulation process. There was obvious FITC fluorescence observed from HeLa cells that incubated with Zn^{2+} pretreated A-DNA nanomachine (Fig. 4C, A-DNA nanomachine), which indicated the "false positive" signal due to the response of active DNAzyme to Zn^{2+} before cellular internalization. On the contrary, FITC fluorescence was barely observed from HeLa cells incubated with Zn^{2+} pretreated P-DNA nanomachine (Fig. 4C, P-DNA nanomachine).

To demonstrate the capability of P-DNA nanomachine for detecting changes of Zn^{2+} concentrations in living cells, HeLa cells were loaded with P-DNA nanomachine, irradiated with NIR light, and further treated with different concentrations Zn^{2+} and pyrithione, to mimic the natural changes of Zn^{2+} levels under physiological stimuli. The intensity of FITC fluorescence recovery at 540 nm gradually increased with Zn^{2+} loading concentration, while UCNPs luminance at 450 nm as an internal standard remained the same (Fig. 5A). The intensity ratio of FITC fluorescence at 540 nm and UCNPs luminance at 450 nm (I_{540}/U_{450}) was also calculated from CLSM images (Fig. 5B). To further verify the accuracy of P-DNA nanomachine for cell imaging, we determined the intracellular amount of Zn^{2+} by ICP-OES [18,40], and the quantification results (Fig. 5C) were well consistent with I_{540}/U_{450} tendency from P-DNA nanomachine (Fig. 5B). This result confirms the NIR activatable P-DNA nanomachine could monitor the concentrations variation of intracellular Zn^{2+}, which has potential applications in monitoring physiological and pathological processes.

4. Conclusions

In conclusion, a NIR activatable P-DNA nanomachine was constructed for spatiotemporally controlled Zn^{2+} imaging in cancer cells. P-DNA nanomachine was composed of UCNPs modified with energy collector FITC, photo-locked DNAzyme strand and its corresponding substrate strands labelled with BHQ1. Part of the UCNPs emission at 450 nm was collected by FITC and quenched by BHQ1 originally via two continuous LRET processes. 980 nm NIR irradiation activated the photo-locked DNAzyme response to Zn^{2+}, resulted in FITC fluorescence recovery at 540 nm while UCNPs luminance at 450 nm remained the same. The as-prepared P-DNA nanomachine achieved operation activation and imaging via single NIR irradiation at 980 nm, and was successfully used to detect Zn^{2+} concentration changes in living cells. The as-presented NIR activatable DNA nanomachine would provide a potential platform for *in vivo* imaging.

CRediT authorship contribution statement

Yuetong Li: Modify experiment procedure, perform experiments, analyze data, Writing – original draft. **Yuxin Xie:** Perform experiments,

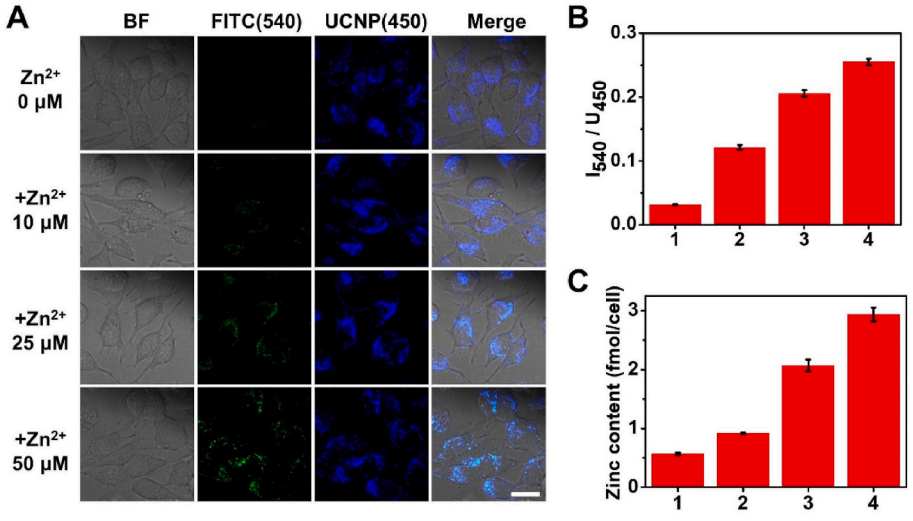

Fig. 5. Intensity of intracellular imaging according to Zn^{2+} concentration. (A) CLSM images of HeLa cells incubated with P-DNA nanomachine in the presence of NIR irradiation and further incubated with different concentrations of Zn^{2+} (scale bar: 20 μm). (B) Normalized FITC fluorescence recovery over UCNP luminance (I_{540}/U_{450}) in (A): 0 μM Zn^{2+} (1); 10 μM Zn^{2+} (2); 25 μM Zn^{2+} (3); 50 μM Zn^{2+} (4). (C) Zinc content measured by ICP-OES for HeLa cells treated with 0 μM Zn^{2+} (1); 10 μM Zn^{2+} (2); 25 μM Zn^{2+} (3); 50 μM Zn^{2+} (4). Data are represented as means ± SD (n = 3).

analyze data. **Yue Zhang:** Design experiment procedure, perform part of experiments. **Hongxia Zhao:** Perform part of experiments. **Huangxian Ju:** Provide suggestions during experiment process. **Ying Liu:** Supervise project, design experiment procedure, analysis data, write and revise manuscript.

Declaration of competing interest

The authors declare that they have no known competing financial interests or personal relationships that could have appeared to influence the work reported in this paper.

Data availability

Data will be made available on request.

Acknowledgements

We gratefully acknowledge the National Natural Science Foundation of China (22022405, 21974064), Natural Science Foundation of Jiangsu Province for distinguished Young Scholars (BK20200010).

Appendix A. Supplementary data

Supplementary data to this article can be found online at https://doi.org/10.1016/j.aca.2022.340149.

References

[1] Y. Chen, C. Mao, Putting a brake on an autonomous DNA nanomotor, J. Am. Chem. Soc. 126 (2004) 8626–8627.
[2] J. Bath, A.J. Turberfield, DNA nanomachines, Nat. Nanotechnol. 2 (2007) 275–284.
[3] L. Yang, J. Fang, J. Li, X. Ou, L. Zhang, Y. Wang, Z. Weng, G. Xie, An integrated fluorescence biosensor for microRNA detection based on exponential amplification reaction-triggered three-dimensional bipedal DNA walkers, Anal. Chim. Acta 1143 (2021) 157–165.
[4] S. Liu, K. Xiang, C. Wang, Y. Zhang, G.C. Fan, W. Wang, H. Han, DNA nanotweezers for biosensing applications: recent advances and future prospects, ACS Sens. 7 (2022) 3–20.
[5] B. Li, J. Liu, H. Zhou, Amplified fluorescence detection of serum prostate specific antigen based on metal-dependent DNAzyme assistant nanomachine, Anal. Chim. Acta 1008 (2018) 96–102.
[6] J. Liu, M. Cui, H. Zhou, W. Yang, DNAzyme based nanomachine for in situ detection of MicroRNA in living cells, ACS Sens. 2 (2017) 1847–1853.
[7] K. Chen, Q. Huang, T. Fu, G. Ke, Z. Zhao, X. Zhang, W. Tan, MicroRNA-initiated and intracellular Na+-Fueled DNAzyme motor for differentiating molecular subtypes of nonsmall cell lung cancer, Anal. Chem. 92 (2020) 7404–7408.
[8] S. Khan, B. Burciu, C.D.M. Filipe, Y. Li, K. Dellinger, T.F. Didar, DNAzyme-based biosensors: immobilization strategies, applications, and future prospective, ACS Nano 15 (2021) 13943–13969.
[9] M. Xu, D. Tang, Recent advances in DNA walker machines and their applications coupled with signal amplification strategies: a critical review, Anal. Chim. Acta 1171 (2021), 338523.
[10] J. Liu, M. Cui, H. Zhou, W. Yang, DNAzyme based nanomachine for in situ detection of MicroRNA in living cells, ACS Sens. 2 (2017) 1847–1853.
[11] P. Wu, K. Hwang, T. Lan, Y. Lu, A DNAzyme-gold nanoparticle probe for uranyl ion in living cells, J. Am. Chem. Soc. 135 (2013) 5254–5257.
[12] L. Li, J. Feng, Y. Fan, B. Tang, Simultaneous imaging of Zn2+ and Cu2+ in living cells based on DNAzyme modified gold nanoparticle, Anal. Chem. 87 (2015) 4829–4835.
[13] H. Si, R. Sheng, Q. Li, J. Feng, L. Li, B. Tang, Highly sensitive fluorescence imaging of Zn2+ and Cu2+ in living cells with signal amplification based on functional DNA self-assembly, Anal. Chem. 90 (2018) 8785–8792.
[14] K. Hwang, P. Wu, T. Kim, L. Lei, S. Tian, Y. Wang, Y. Lu, Photocaged DNAzymes as a general method for sensing metal ions in living cells, Angew. Chem. Int. Ed. 53 (2014) 13798–13802.
[15] W. Wang, N.S.R. Satyavolu, Z. Wu, J.R. Zhang, J.J. Zhu, Y. Lu, Near-infrared photothermally activated DNAzyme-gold nanoshells for imaging metal ions in living cells, Angew. Chem. Int. Ed. 56 (2017) 6798–6802.
[16] Z. Yang, K.Y. Loh, Y.T. Chu, R. Feng, N.S.R. Satyavolu, M. Xiong, S.M. Nakamata Huynh, K. Hwang, L. Li, H. Xing, X. Zhang, Y.R. Chemla, M. Gruebele, Y. Lu, Optical control of metal ion probes in cells and zebrafish using highly selective DNAzymes conjugated to upconversion nanoparticles, J. Am. Chem. Soc. 140 (2018) 17656–17665.
[17] L. Xiao, C. Gu, Y. Xiang, Orthogonal activation of RNA-cleaving DNAzymes in live cells by reactive oxygen species, Angew. Chem. Int. Ed. 58 (2019) 14167–14172.
[18] D. Yi, J. Zhao, L. Li, An enzyme-activatable engineered DNAzyme sensor for cell-selective imaging of metal ions, Angew. Chem. Int. Ed. 60 (2021) 6300–6304.
[19] X. Wang, X. Yi, Z. Huang, J. He, Z. Wu, X. Chu, J.H. Jiang, "Repaired and activated" DNAzyme enables the monitoring of DNA alkylation repair in live cells, Angew. Chem. Int. Ed. 60 (2021) 19889–19896.
[20] Q. Wang, K. Tan, H. Wang, J. Shang, Y. Wan, X. Liu, X. Weng, F. Wang, Orthogonal demethylase-activated deoxyribozyme for intracellular imaging and gene regulation, J. Am. Chem. Soc. 143 (2021) 6895–6904.
[21] J. Zhao, J. Gao, W. Xue, Z. Di, H. Xing, Y. Lu, L. Li, Upconversion luminescence-activated DNA nanodevice for ATP sensing in living cells, J. Am. Chem. Soc. 140 (2018) 578–581.
[22] J. Zhao, H. Chu, Y. Zhao, Y. Lu, L. Li, A NIR light gated DNA nanodevice for spatiotemporally controlled imaging of MicroRNA in cells and animals, J. Am. Chem. Soc. 141 (2019) 7056–7062.
[23] M. Ye, Y. Kong, C. Zhang, Y. Lv, S. Cheng, D. Hou, Y. Xian, Near-infrared light controllable DNA walker driven by endogenous adenosine triphosphate for in situ spatiotemporal imaging of intracellular MicroRNA, ACS Nano 15 (2021) 14253–14262.
[24] J. Zhao, Y. Li, M. Yu, Z. Gu, L. Li, Y. Zhao, Time-resolved activation of pH sensing and imaging in vivo by a remotely controllable DNA nanomachine, Nano Lett. 20 (2020) 874–880.
[25] C.Y. Li, B. Zheng, Y.F. Kang, H.W. Tang, D.W. Pang, Integrating 808 nm light-excited upconversion luminescence powering with DNA tetrahedron protection: an exceptionally precise and stable nanomachine for intracelluar MicroRNA tracing, ACS Sens. 5 (2020) 199–207.
[26] B. Kumar, K. Malhotra, R. Fuku, J. Van Houten, G.Y. Qu, P.A.E. Piunno, U.J. Krull, Recent trends in the developments of analytical probes based on lanthanide-doped upconversion nanoparticles, TrAC, Trends Anal. Chem. 139 (2021), 116256.
[27] M.S. Arai, A.S.S. de Camargo, Exploring the use of upconversion nanoparticles in chemical and biological sensors: from surface modifications to point-of-care devices, Nanoscale Adv. 3 (2021) 5135–5165.
[28] C. Liu, L. Chang, H. Wang, J. Bai, W. Ren, Z. Li, Upconversion nanophosphor: an efficient phosphopeptides-recognizing matrix and luminescence resonance energy transfer donor for robust detection of protein kinase activity, Anal. Chem. 86 (2014) 6095–6102.
[29] F. Zhou, U.J. Krull, Spectrally matched duplexed nucleic acid bioassay using two-colors from a single form of upconversion nanoparticle, Anal. Chem. 86 (2014) 10932–10939.
[30] X. Zhang, W. Chen, X. Xie, Y. Zhang, Z. Chao, H. Ma, Y. Liu, H. Ju, energy pumping by surface collectors on upconversion nanoparticles for extended transfer and efficient self-evaluable photodynamic therapy, CCS Chem. (2021) 1510–1521.
[31] Y. Zhang, Y. Zhang, X. Zhang, Y. Li, Y. He, Y. Liu, H. Ju, A photo zipper locked DNA nanomachine with an internal standard for precise miRNA imaging in living cells, Chem. Sci. 11 (2020) 6289–6296.
[32] Y. Li, X. Zhang, Y. Zhang, Y. Zhang, Y. He, Y. Liu, H. Ju, Activatable photodynamic therapy with therapeutic effect prediction based on a self-correction upconversion nanoprobe, ACS Appl. Mater. Interfaces 12 (2020) 19313–19323.
[33] Y. Fang, Y. Li, Y. Li, R. He, Y. Zhang, X. Zhang, Y. Liu, H. Ju, In situ protease secretion visualization and metastatic lymph nodes imaging via a cell membrane-anchored upconversion nanoprobe, Anal. Chem. 93 (2021) 7258–7265.
[34] C.J. Frederickson, J.Y. Koh, A.I. Bush, The neurobiology of zinc in health and disease, Nat. Rev. Neurosci. 6 (2005) 449–462.
[35] A. Takeda, H. Tamano, M. Tochigi, N. Oku, Zinc homeostasis in the hippocampus of zinc-deficient young adult rats, Neurochem. Int. 46 (2005) 221–225.
[36] K.P. Carter, A.M. Young, A.E. Palmer, Fluorescent sensors for measuring metal ions in living systems, Chem. Rev. 114 (2014) 4564–4601.
[37] X. Zhang, W. Chen, X. Xie, Y. Li, D. Chen, Z. Chao, C. Liu, H. Ma, Y. Liu, H. Ju, Boosting luminance energy transfer efficiency in upconversion nanoparticles with an energy-concentrating zone, Angew. Chem. Int. Ed. 58 (2019) 12117–12122.
[38] H. Dong, L.D. Sun, W. Feng, Y. Gu, F. Li, C.H. Yan, Versatile spectral and lifetime multiplexing nanoplatform with excitation orthogonalized upconversion luminescence, ACS Nano 11 (2017) 3289–3297.
[39] G. Niu, R. Zhang, X. Shi, H. Park, S. Xie, R.T.K. Kwok, J.W.Y. Lam, B.Z. Tang, AIE luminogens as fluorescent bioprobes, TrAC, Trends Anal. Chem. 123 (2020), 115769.
[40] H. Wang, Y. Chen, H. Wang, X. Liu, X. Zhou, F. Wang, DNAzyme-loaded metal-organic frameworks (MOFs) for self-sufficient gene therapy, Angew. Chem. Int. Ed. 58 (2019) 7380–7384.